Electronic Supplementary Information

Asymmetric Gel Polymer Electrolyte with High Lithium Ionic Conductivity for Dendrite-free Lithium Metal Batteries

Linge Li[ab], Mingchao Wang[c], Jian Wang[a], Fangmin Ye[d], Shaofei Wang[e], Yanan Xu[f], Jingyu Liu[f], Guoguang Xu[a], Yue Zhang[ab], Yongyi Zhang[ag], Cheng Yan[f], Nikhil V. Medhekar[c], Meinan Liu[ag]*, Yuegang Zhang[ah]

[a] *i-Lab, Suzhou Institute of Nano-Tech and Nano-Bionics, Chinese Academy of Sciences, Suzhou, 215123, China.*

[b] *Nano Science and Technology Institute, University of Science and Technology of China, Suzhou, 215123, China.*

[c] *Department of Materials Science and Engineering, Monash University, Clayton, VIC 3800, Australia.*

[d] *School of Science, Zhejiang Sci-Tec University, Hangzhou 310000, China.*

[e] *Department of Chemical Engineering, University of Rochester, Rochester, New York 14627, USA.*

[f] *School of Chemistry, Physics and Mechanical Engineering, Queensland University of Technology, Brisbane, QLD 4001, Australia.*

[g] *Division of Nanomaterials and Jiangxi Key Lab of Carbonene Materials, Suzhou Institute of Nano-Tech and Nano-Bionics, Nanchang, Chinese Academy of Sciences, Nanchang 330200, China.*

[h] *Department of Physics, Tsinghua University, Beijing 100084, China.*

* Corresponding author. *E-mail address:* mnliu2013@sinano.ac.cn

Supporting Figures

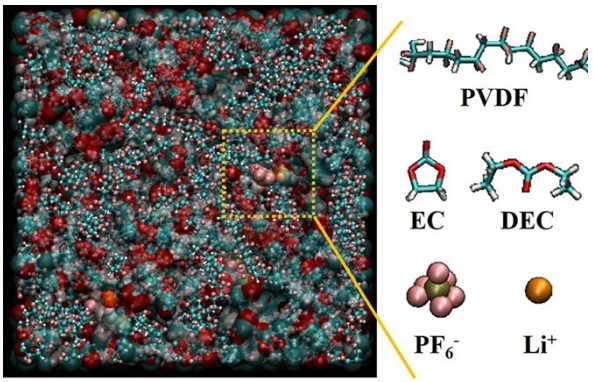

Fig. S1 Atomistic structures of PVDF-$LiPF_6$ system including all the components of PVDF matrix, EC and DEC solvents, and $LiPF_6$ salt.

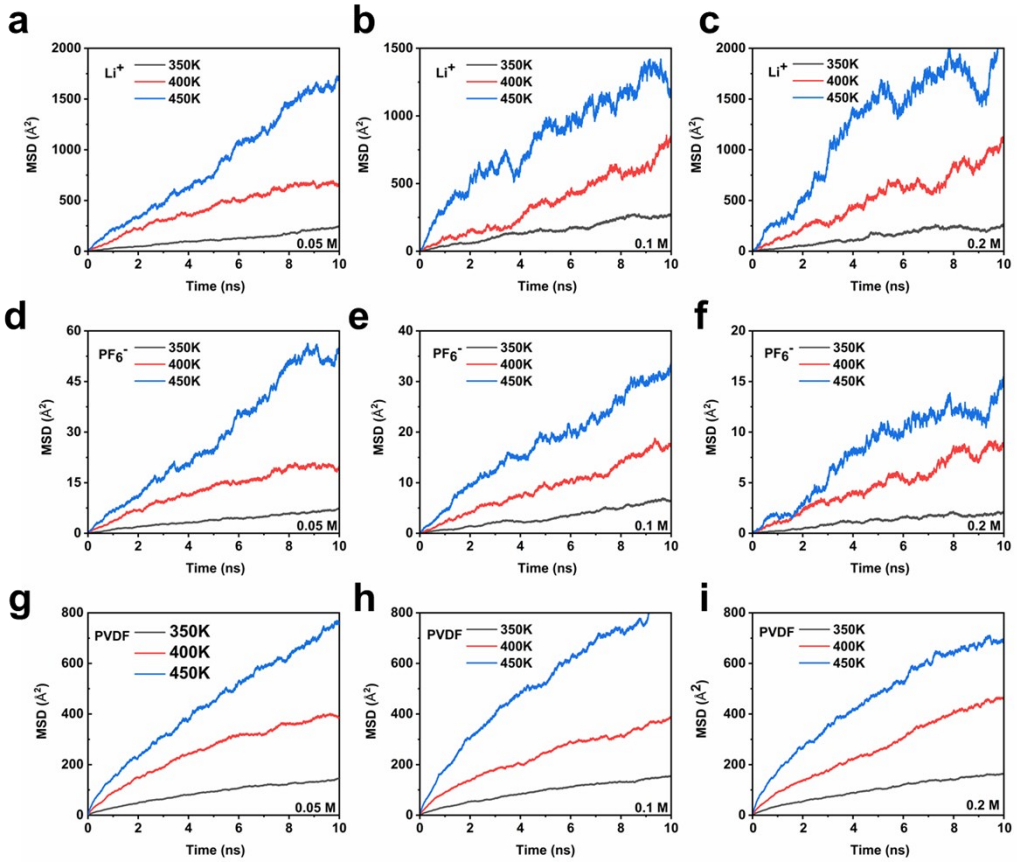

Fig. S2 The mean square displacements (MSDs) of Li^+ and PF_6^- ions at the salt concentrations of 0.05 M, 0.1 M and 0.2 M.

Mechanical properties of PVDF-HFP membranes

Excellent mechanical properties are highly demanded for electrolyte membrane considering the safety concern and cell assembly technique. Owing to the continuous polymer matrix of channel structure, Asymmetric GPE exhibits good mechanical integrity and self-standing capability; while Porous GPE fails to support its own weight and tends to entangle itself. The mechanical properties of these two membranes was furhter investigated and summarized in Fig.S3 and Table S1. As shown in Fig. S3a, the stress-strain curve of asymmetric membrane shows linear elastic response before plastic deformation and final fracture strain over 100%, indicating its outstanding stretchability, but the fracture strain of porous membrane is only 3.5%. Young's modulus of asymmetric membrane is calculated to be 53 MPa, which is also much higher than that of porous membrane (33 MPa). Nanoindentation technique also used here to identify the mechanical properties of membranes in the vertical direction. As the results shown in Fig. S3b and Table S1, the asymmetric membrane shows an elastic modulus of 58 MPa and hardness of 2 MPa in unloading process. By comparison, porous membrane presents more viscoelastic behavior with a lower elastic modulus and hardness of 29 and 0.8 MPa, respectively. The nanoporous sublayer in asymmetric membrane may contribute to its high elastic modulus and hardness, which can facilitate suppressing dendrite growth in Li metal batteries. All the above results demonstrate the outstanding stiffness and toughness of asymmetric membrane, which will improve the safety of LMBs.

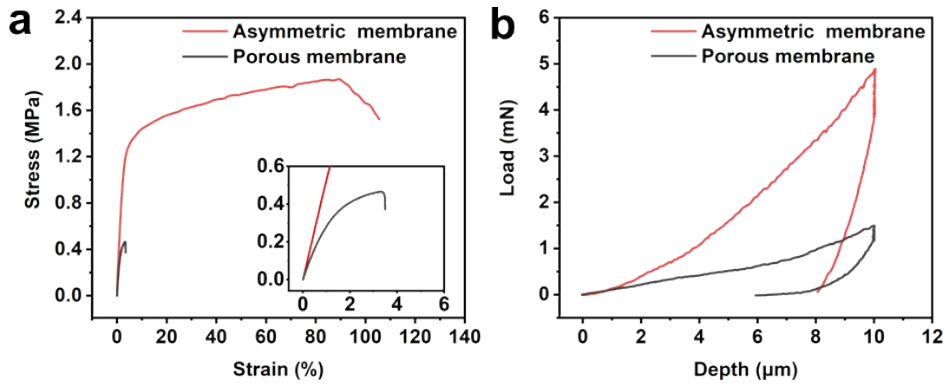

Fig. S3 (a) Stress-strain curves of asymmetric and porous PVDF-HFP membranes. (b) Typical load-depth curves obtained on the bottoms of asymmetric and porous PVDF-HFP membranes.

Table S1 Mechanical properties of different PVDF-HFP membranes

Samples	Tensile modulus (MPa)	Tensile strength (MPa)	Maximum strain (%)	Reduced modulus (MPa)	Hardness (MPa)
Asymmetric membrane	53.18	1.87	105.50	57.8	1.9
Porous membrane	32.99	0.46	3.50	28.9	0.8

Crystallization information of PVDF-HFP membranes

The crystal structure of PVDF-HFP with different morphologies was studied by XRD. As shown in Fig. S4, characteristic diffraction peaks at 20.26°, 36.2°, and 41.3° in asymmetric membrane, can be attributed to (110), (001), and (400) planes of PVDF-HFP with β-phase. While porous membrane shows typical α-phase, as evidenced by strong diffraction peaks at 18.5°, 19.9°, and 26.6°, attributed to (020), (110) and (021) planes of α-phase, respectively. Furthermore, asymmetric membrane also shows relatively lower crystallinity (29.14%) compared to porous membrane (35.27%), as calculated from DSC curves (Fig. S5 and Table S2). It can be found two endothermic peaks in asymmetric membrane. The first peak at 150.3 °C can be attributed to phase transformation and recrystallization of PVDF-HFP polymer, and the second one at 162.0 °C corresponds to its melting behavior. While in porous membrane, there is only one endothermic peak at 158.7 °C, which is caused by the slow crystallization in preparing process. From the peak area, it can be deduced that the crystallinity of porous membrane is higher than that of asymmetric membrane, which is well matching with XRD and SEM results. The polar β-phase with high dielectric constant in asymmetric membrane may promote the dissociation of lithium salt in organic solvent, hence increasing the concentration of ions.

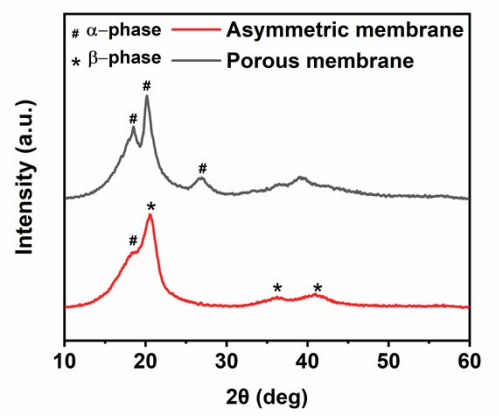

Fig. S4 XRD patterns of Asymmetric and Porous PVDF-HFP membranes.

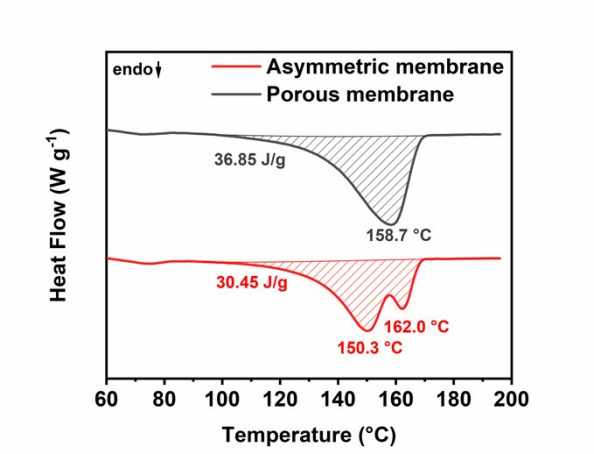

Fig. S5 DSC curves and melting enthalpy of Asymmetric and Porous PVDF-HFP membranes.

Table S2 Melting enthalpy (*ΔH)* and degree of crystallization (*Xc*) of PVDF-HFP membranes.

Samples	*ΔH* ($J \cdot g^{-1}$)	Crystallinity (%)
Asymmetric membrane	30.45	29.14
Porous membrane	36.85	35.27

Table S3 Membrane parameters of Celgard and PVDF-HFP membrane

	Thickness (μm)	Density ($g \cdot cm^{-3}$)	Areal density ($mg \cdot cm^{-2}$)	Porosity (%)
Asymmetric membrane	120	0.27	3.24	88
Porous membrane	120	0.40	4.84	71
Celgard 2325	25	0.60	1.50	53

Table S4 Ionic transport properties of GPEs and Celgard with liquid electrolyte (at 20 °C)

	Electrolyte uptake (%)	Ionic conductivity (mS cm^{-1})	Li^+ transference number	Tortuosity
Asymmetric GPE	472	3.36	0.66	0.96
Porous GPE	165	2.22	0.65	1.07
Celgard+LE	103	0.95	0.34	1.41

Electrochemical stabilties of GPEs

The electrochemical stabities of GPEs were studied by linear sweep voltammetry (LSV). As shown in Fig. S6, the increase of the oxidation current can be observed for Asymmetric GPE at 4.7 V and Porous GPE at 4.3 V, indicating that Asymmetric GPE suppresses the oxidative decomposition of electrolyte compared with Porous GPE.

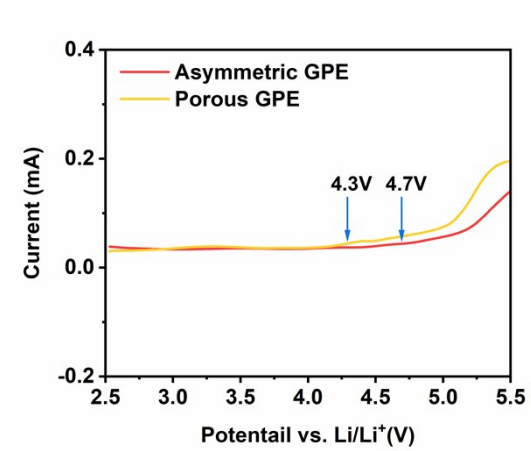

Fig. S6 LSV curves of Asymmetric GPE and Porous GPE with a scan rate of 10 mV s^{-1}.

The role of channel layer and nanoporous layer in Asymmetric GPE

Two electrochemically deposited Li experiments using Li|Asymmetric GPE|Cu system were designed to study the influence of these two layers. One is channel layer cotacting Cu and the other is nanoporous layer contacting Cu. The electrodeposition current and capacity are 0.5 mA cm-2 and 1 mAh cm-2, respectively. The morphology of Cu surface after electrodepositing Li is shown in Fig. R3. It can be found the one contacting channel layer presents rough surface; while the one contacting

nanoporous layer shows smooth layer, suggesting that nanoporous layer plays a significant role in suppress the growth of lithium dendrites through redistributing ionic flux and reduceing the current density. As a consequence, these two different structures indeed play different roles.

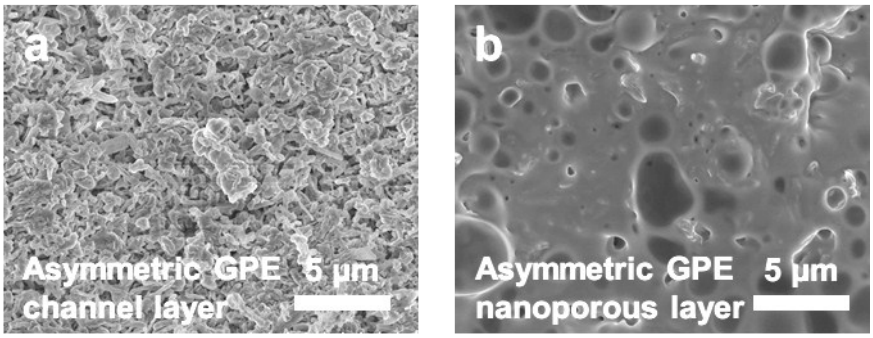

Fig. S7 SEM images of lithium electrodeposited on Cu foils with a) channle layer attaching, b) nanoporous layer attaching.

Performance of Porous GPE in lithium metal cells

Firstly, we evaluated the Li deposition process using Li|Porous GPE|Cu cells. As shown in Fig. S8a, the morphology of electrodeposited Li on Cu foils presents rough surface with short dendrites, which is very different from the smooth surface with round cobble using Asymmetric GPE in Fig. S8b. Furthermore, in Fig. S9a , it can be found that the short-circuit appears in Li|Li cells using Porous GPE after 183 h cycling at operation of 1 mA cm^{-2} and 1 mAh cm^{-2}; while Li|Li cells using Asymmetric GPE keeps stable over 250 h cycling under same operation condition. These results well demonstrate that Porous GPE with pore size of 5-10 μm cannot effectively suppress the growth of lithium dendrites compared with Asymmetric GPE.

Furthermore, we also applied this Porous GPE in Li|LFP cell. It can be found that Porous GPE cell delivers a similar discharge capacity to Asymmetric GPE cell in the initial 30 cycles. After that, the discharge capacity becomes unstable, and it even drops to zerofail at 38 cycles. Additionally, the Coulombic efficiency jumps up and down after 15 cycles. These behaviors indicate that short circuit

occurs in the Porous GPE cell. The main reason may be caused by the poor mechanical property of Porous GPE leading to the micro-inner short circuit in Porous GPE cells.

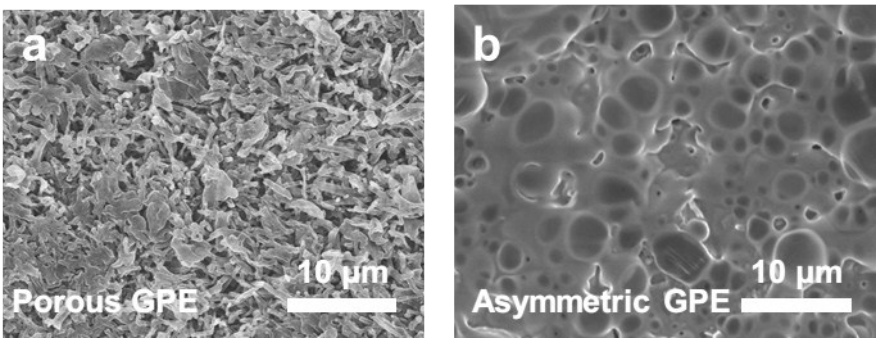

Fig. S8 SEM images of lithium electrodeposited on Cu foils with (a) Porous GPE and (b) Asymmetric GPE for 1 mAh cm^{-2} at 0.5 mA cm^{-2}.

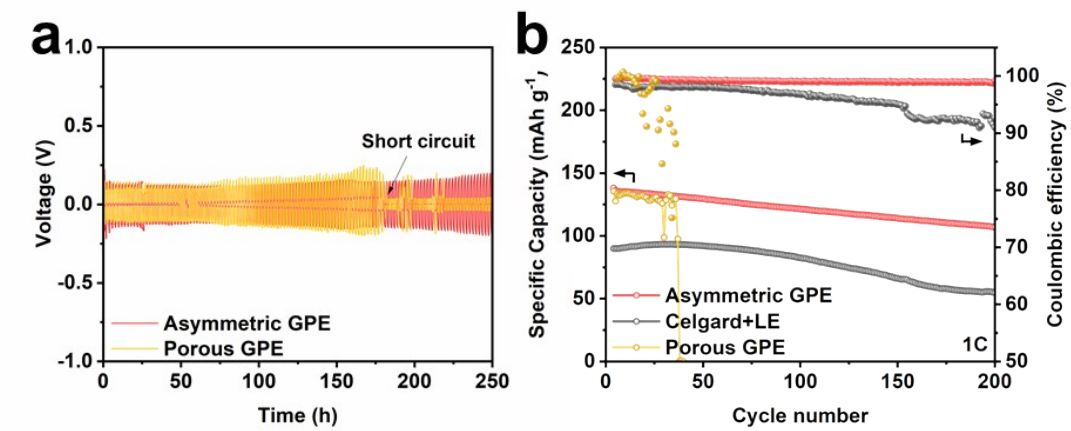

Fig. S9 (a) Voltage stability of the Li|Li symmetric cells and (b) cycling performances at 1 C of LFP cells.

The influence of electroly amount in liquid electrolyte system

Electrolyte amount is a key parameter in the practical application. In Chen's report, they commented that almost 100 μL electrolyte is used in coin-cell test with the cathode loading of 1 mAh (Critical parameters for evaluating coin cells and pouch cells of rechargeable Li-metal batteries. Joule, 2019, 3(4): 1094-1105). In this work, we set $\mu L_{LE}/mg_{LFP}$ to 10. In our coin cells, 47 μL liquid electrolyte was used, which is equal to the absorption amount of one piece of GPE membrane, but much less than the general used amount of 80-100 μL in most reported works. To verify the influence of electrolyte

amount on the performance of Li/LFP cells, 80 μL liquid electrolyte has also been demonstrated here. As shown in Fig. S10, it can be found the capacity can be greatly enhanced with liquid electrolyte volume increasing from 47 to 80 μL. But the capacity values are still lower than the values contributed by Asymmetric GPE. As a consequence, our Asymmetric GPE indeed delivers excellent performance.

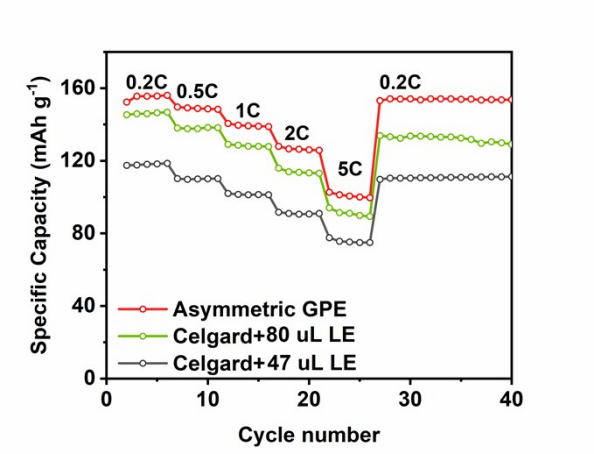

Fig. S10 Rate performances of LFP cells with GPE and Celgard+LE.

Table S5 Comparation of GPE and GPE cell performances.

Gel electrolyte	Ionic conductivity (mS cm^{-1})	Li^+ transference number	Specific capacity of Li/LFP cells (mAh g^{-1})					Reference
			0.2 C	0.5 C	1 C	2 C	5 C	
Asymmetric GPE	**3.36 @20 °C**	**0.66**	**156**	**149**	**140**	**127**	**101**	**This work**
es-PVPSI	0.68 @25 °C	0.85	140	-	107	94	-	*Adv. Energy Mater.*, 2019, 9(10): 1803422.
PVDF-HFP/IL	0.88 @25 °C	-	145	133	123	-	91	*Nano Energy*, 2018, 54: 17-25.
PVDF/TiO_2/IL	0.74 @25 °C	0.12	145	122	50	14	-	*Nano Energy*, 2018, 47: 35-42.
PVDF-HFP/LLZO	0.11 @25 °C	0.61	123	113	104	83	-	*Nano Energy*, 2018, 45: 413-419.
PEGDA/ETPTA 3D-GPE	0.56 @25 °C	-	133	127	103	-	-	*Adv. Sci.*, 2018, 5(9): 1800559.
3D-GPE	2.36 @25 °C	-	-	151	140	124	-	*Adv. Mater.*, 2017, 29(13): 1604460.
ipn-PEA	0.22 @25 °C	0.65	-	141	131	112	66	*J. Am. Chem. Soc.*, 2016, 138(49): 15825-15828.
PECA	2.7 @20 °C	0.45	155	145	140	120		*ACS Appl. Mater. Interfaces,* 2017, 9(10): 8737-8741.
PVDF–NWF	0.30 @25 °C	0.43	129	115	78	-	-	*Energy Environ. Sci.*, 2013, 6(2): 618-624.